

Optical feedback-induced spatiotemporal patterns with power law spectra in a liquid crystal light valve

PEDRO J. AGUILERA-ROJAS, MARCEL G. CLERC,  AND SIMON NAVIA* 

Departamento de Física and Millennium Institute for Research in Optics, Facultad de Ciencias Físicas y Matemáticas, Universidad de Chile, Casilla 487-3, Santiago, Chile

*simon.navia.sn@gmail.com

Received 5 March 2024; revised 18 May 2024; accepted 19 May 2024; posted 21 May 2024; published 3 June 2024

Pattern formation can be induced by coupling electromagnetic fields to a polarizable and lossy medium. Increasing energy injection patterns can exhibit aperiodic behaviors. We investigate the self-organization of unidimensional aperiodic patterns. Based on a liquid crystal light valve (LCLV) with optical feedback, we observed aperiodic one-dimensional patterns with power laws in the temporal and spatial spectrum density of the light intensity, and their pseudo envelope and phase characteristic of spatiotemporal complexity. Theoretically, a local model describes the system close to nascent bistability and spatial instability. Numerical simulations of this model show chaotic spatiotemporal patterns whose temporal and spatial spectra have exponents similar to those observed experimentally. © 2024 Optica Publishing Group

<https://doi.org/10.1364/OL.522830>

Non-equilibrium processes often lead to the emergence of patterns, which evolve from a homogeneous state by spontaneously breaking spatial symmetry [1,2]. In optics, coupling an electromagnetic field to a polarizable medium and losses can induce a diffraction–diffusion mechanism of pattern formation [3]. For example, transverse patterns have been observed in gas [4,5] and semiconductor laser [6], photorefractive media (see the textbook [7] and reference therein), sodium vapor [8] and liquid crystal cells [9] with single-mirror feedback, and liquid crystal light valve (LCLV) with optical feedback [10], to mention a few. As one injects energy, secondary instabilities can generate oscillations and complex spatiotemporal behaviors of optical patterns [5,11]. Dissipative systems far from equilibrium can exhibit non-periodic spatiotemporal dynamics. These include fiber lasers [12,13], nonlinear optics [14,15], active matter [16], interfacial dynamics [17], chemical reactions [18], financial markets [19], and Bose–Einstein condensates [20], among others. In all of these systems, the observed dynamics from a statistical perspective are *turbulent-like*, i.e., unpredictable (spatiotemporal chaos), and a wide range of spatial wavelengths participate in the permanent dynamics (power law spectra). The power law spectrum density has been observed for different quantities such as kinetic energy, light intensity, information, intensity correlation, and phase gradient. A pioneering example of this type of behavior is the phase turbulence [21]. In most of the previous systems where turbulence-like behavior is observed, a power law

is typically observed for a decade or a few decades of wavenumber in the spectrum due to the absence of different structures or defects at different scales [12–20]. Spatiotemporal complexity of fingerprint patterns with turbulent-like behavior has recently been observed in an LCLV with optical feedback [15].

This Letter aims to investigate spatiotemporal self-organization behaviors for one-dimensional aperiodic optical patterns. Based on a liquid crystal light valve with optical feedback and a spatial light modulator, we observe aperiodic one-dimensional patterns (see Fig. 1) when one increases the intensity of the illumination light or the free propagation length L of the optical feedback. The temporal and spatial intensity spectral densities exhibit power laws. The pattern's dynamical behavior is characterized by determining its pseudo envelope and phase using the Hilbert transform [22]. This pseudo phase field exhibits spatial and temporal spectra with power laws. The phase exhibits k^{-2} and ω^{-2} spectra, which are typical of phase turbulence [21]. The amplitude (light intensity) and pseudo envelope of the pattern spatial and temporal spectral density show defect turbulence with an exponent close to -3 and -2 , respectively. The structure functions of the amplitude fluctuations at different exponents allow us to conclude that the observed dynamics are self-similar. Theoretically, close to the nascent bistability and spatial instability, *Lifshitz point*, a local model describes the system. Numerical simulations of this model present spatiotemporal chaotic patterns [23]. The numerically observed dynamics are characterized by complex defect dynamics, whose temporal and spatial spectra tend to follow power laws. The envelope and phase of the observed patterns are characterized by spatial and temporal spectra with similar exponents to those observed experimentally.

The LCLV with optical feedback is a flexible setup that exhibits a wide range of dynamic behaviors, such as multistability, front propagation, pattern formation, localized states, and aperiodic spatiotemporal dynamics (see Ref. [10] and references therein). Figure 1(a) shows a schematic representation of the setup. The LCLV consists of a nematic liquid crystal LC-654 (NIOPIK) with a dielectric anisotropy constant $\epsilon_a = 10.7 \epsilon_0$ sandwiched between two glass layers separated by a distance $d = 15 \mu\text{m}$. To apply an electrical voltage to the liquid crystals, transparent indium tin oxide (ITO) electrodes and a photoconductive layer are deposited on the glasses. The back layer of the liquid crystal cell contains a dielectric Bragg mirror with optimized reflectivity for 632.8 nm light. The molecules on the

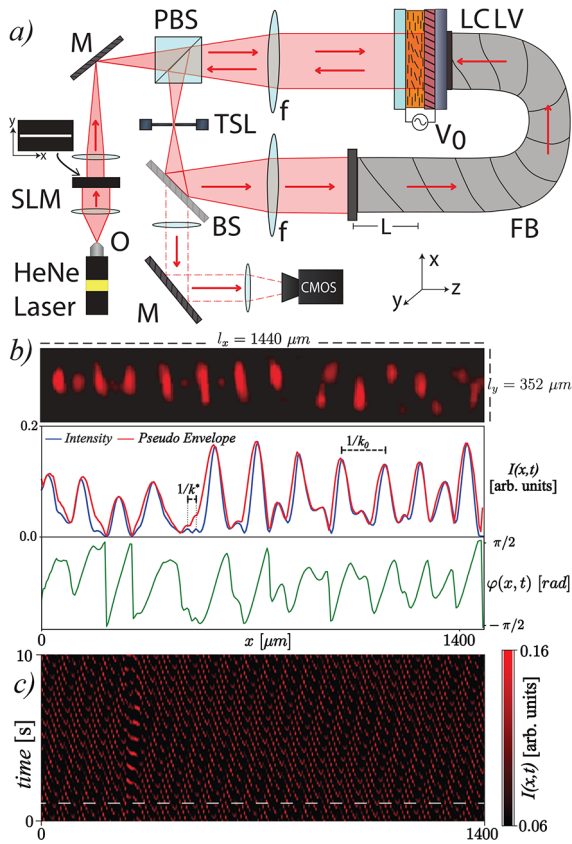


Fig. 1. Experimental aperiodic patterns in a liquid crystal light valve with optical feedback. (a) Schematic liquid crystal light valve (LCLV) representation with optical feedback. The setup is composed of a coherent light source (He–Ne laser) sent through a spatial light modulator (SLM) and a polarizing beam splitter (PBS) before hitting the LCLV. After reflection, the light is filtered in a transversal slit (TSL) placed in the Fourier plane, and then the light is brought to the fiber bundle (FB) with a beam splitter (BS) and to a complementary metal–oxide–semiconductor (CMOS) with a mirror (M). f represents achromatic lenses, and L is the free propagation length. The applied voltage of the LCLV is $V_0 = 9.72$ Vrms. The red arrows indicate the propagation of light. The illuminated region of the LCLV is a quasi-one-dimensional region of dimensions $1440 \times 352 \mu\text{m}^2$. (b) Snapshot and middle plane profile (pattern intensity and their pseudo envelope and phase φ) of a one-dimensional pattern in which different colors account for different average inclinations of liquid crystal molecules. k_0 and k^* are the pattern and characteristic coupling wavenumber ($k_0 < k^*$). (c) Spatiotemporal evolution of one-dimensional patterns.

cell wall are anchored parallel to it, corresponding to a planar anchoring in the cell’s diagonal direction. The LCLV can be electrically addressed by applying an oscillatory voltage V_0 Vrms and a frequency $f_0 = 1.0$ kHz across the layer. The optical valve is optically forced with a He–Ne laser of intensity I_{in} and wavelength $\lambda_0 = 632.8$ nm. The LCLV is placed in a $4f$ optical configuration ($f = 25$ cm) as shown in Fig. 1(a). A transversal slit (TSL) is placed in the Fourier plane to filter spatial modes. The optical feedback circuit is closed with a fiber bundle (FB) placed $4f$ from the LCLV front surface. Depending on the local light intensity, the optical fiber bundle injects the light into the photoconductive layer and applies an additional local voltage to the liquid crystal material. The

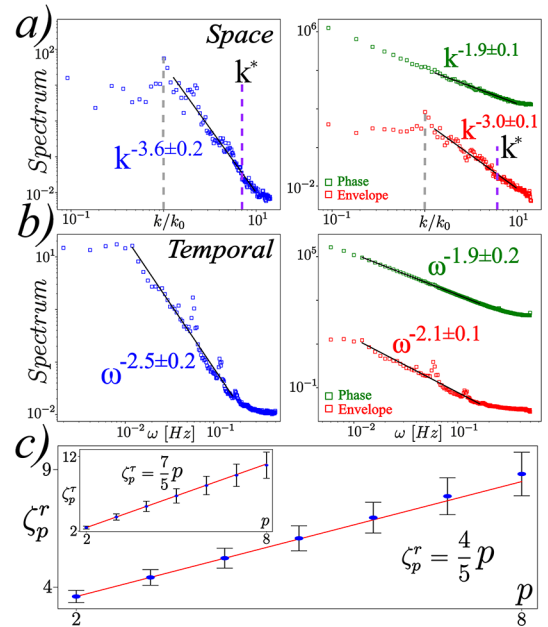


Fig. 2. Experimental spatiotemporal complexity of patterns in a liquid crystal light valve with optical feedback. (a) Spatial and (b) temporal spectra of the light intensity $I(x, t)$ (left panel) and pseudo phase and enveloped field (right panel). The points show the experimental results and the straight continuous curves help show the power law trend. Vertical dashed lines account for characteristic wavenumbers. (c) Spatial exponent ζ_p^r of the structure function $S_p(r)$ as a function of the p index. The inset accounts for the temporal exponent ζ_p^r as a function of the p index. The points and their respective error bars are the exponents obtained experimentally. The straight solid lines show the trend of the points.

optical feedback loop is designed so that the light simultaneously undergoes diffraction propagation (characterized by the length L) and polarization interference induced by the polarizing beam splitter (PBS). For one-dimensional experiments of dimensions $l_x = 1440 \mu\text{m}$ and $l_y = 352 \mu\text{m}$, a spatial light modulator (SLM) is considered. The SLM prevents optical feedback in unilluminated areas, thereby creating an absorbing boundary condition. The experiment is monitored by a complementary metal–oxide–semiconductor (CMOS) camera.

Figures 1(b) and 1(c) show a snapshot of a one-dimensional aperiodic pattern with k_0 wavenumber and its respective spatiotemporal evolution. This chart shows that the pattern also exhibits other wavelengths (k^*), which are coupled with the dynamics of the pattern’s global mode (k_0). Likewise, one infers an aperiodic complex dynamics the pattern defects. The patterns observed are chaotic in nature [11]. To characterize the dynamics statistically, we calculate the spatial and temporal spectrum density of light intensity $I(x, t)$ defined in the spatial case by $\langle \int e^{ikx} |I(x, t)|^2 dx \rangle / T$, where x and t stand for the spatial coordinate and time, respectively, k is the wavenumber, and the symbol $\langle \rangle$ accounts for the temporal average in a long period T . The temporal spectrum is defined in a similar manner. Figure 2 shows the spectrum densities obtained, characterized by tails with power laws of approximately $k^{-3.5}$ and $\omega^{-2.5}$. This manifests the spatiotemporal complexity of the patterns [12–20], characterized by the dynamics of defects and coupling of modes with the different wavenumbers, which includes a decade of wavenumber. Note that the liquid crystal is a strongly overdamped waveless

medium. Due to the inherent fluctuations of the experimental system, noise, the spectra for large wavenumbers or frequencies deviate from the power law and tend to flatten out [24].

To understand complex dynamics, the pattern evolution can be decomposed into the pseudo envelope and phase of the patterns using the analytical signal buildup with the Hilbert transform [22,25]. This type of method has been implemented to understand complex patterns in the catalytic oxidation of carbon monoxide [25] and linear [26] and nonlinear optics [15]. Figure 2 shows the spectral density of the pseudo phase and envelope of the pattern. The spectrum of this phase has an exponent close to k^{-2} and ω^{-2} , which is a characteristic of phase turbulence [21]. The origin of this exponent corresponds to non-correlated abrupt transitions between two typical values of the phase. For the pseudo envelope field, we find that the tails of the spectra are close to k^{-3} and ω^{-2} , which accounts for the defect dynamics. In addition, one can study the higher-order correlations, also called *structure functions* [27], to better understand the pattern's dynamics and whether they have characteristic scales. Let us introduce temporal structure functions $S_p(\tau) \equiv \langle \| |I(t) - I(t + \tau)| \|^p \rangle$, where the symbols $\| \|$ and $\langle \rangle$ account for the spatial norm and the temporal average, respectively. For spatial self-similar turbulent fluid dynamics, the Kolmogorov theory predicts a scaling law of type $S_p(\tau) \propto \tau^{\zeta_p^t}$ [27], where ζ_p^t is the exponent of the structure function. Namely, the system does not have characteristic scales in the turbulent window. Analogously, one can introduce spatial structure functions $S_p(r)$. We also expect $S_p(r) \propto r^{\zeta_p^s}$ for temporal self-similar turbulence. Figure 2(c) summarizes the results found. From this chart, we infer that the observed behavior is self-similar.

To account for the experimental observations, we consider the LCLV with optical feedback simultaneously close to the nascent bistability and spatial instability, *the Lifshitz point* [28], the dynamics of the system is described by

$$\partial_t u = \eta + \epsilon u - u^3 - \nu \partial_{xx} u - \partial_{xxx} u + c(\partial_x u)^2 + \kappa u \partial_{xx} u, \quad (1)$$

where the order parameter $u(x, t)$ accounts for the deviation of the average molecular orientation $\theta(x, t)$ with respect to a critical value θ_c and the light intensity I reaching the camera is related to $u(x, t)$ by $I(x, t) \approx I_m(1 - \cos[0.4d\lambda_0 \cos^2(\theta_c)(1 - 2 \tan(\theta_c)u/u_0)])$ with u_0 a normalization constant [28]. ϵ is the bifurcation parameter, which is proportional to the voltage minus the critical one; η is a parameter that controls the size of bistability, which is proportional to the intensity of the input laser; ν is the anti-diffusion coefficient, which is proportional to the elastic diffusion minus the square of the diffraction propagation length; and c and κ account for the nonvariational advection and nonlinear diffusion; both are proportional to the diffraction propagation length. The detailed relationship between the parameters of Eq. (1) and the physical parameters of the LCLV with optical feedback is given in [29].

It is known that model Eq. (1) presents chaotic spatiotemporal patterns [23]. Figure 3(a) shows the typical spatiotemporal chaotic patterns, which present complex defect dynamics. Analogously to the experimental case, we have calculated the spatial and temporal spectrum density of the order parameter u , which is illustrated in Figs. 3(b) and 3(c). In this case, the spectra have many oscillations related to the harmonics of the main wavenumber and frequency. However, the spectra follow a power law trend close to $k^{-3.5}$ and $\omega^{-2.2}$, which are qualitatively in agreement with the experimental observations (see Fig. 2). We have determined

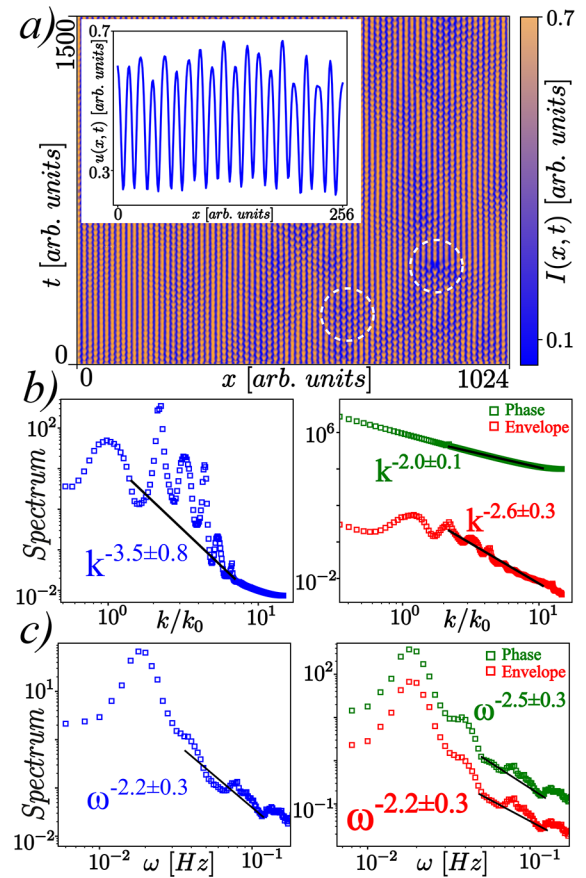


Fig. 3. Numerical spatiotemporal complexity of patterns in model Eq. (1) by $\eta = -0.04$, $\epsilon = -0.092$, $\nu = 1.0$, $c = 10.4$, and $\kappa = -3.05$. (a) Spatiotemporal diagram of the aperiodic pattern. Inset accounts for the profile of an extract of the pattern. Dashed circumferences show defects in the pattern. (b) and (c) Spatial and temporal spectrum density of the order parameter $u(x, t)$ (left panels) and the pseudo phase and envelope field of the pattern (right panels). The points are the results obtained numerically, and the straight lines show the power law trend of the numerical data.

the pseudo envelope and phase field to characterize the observed dynamics analogously to the experimental analysis. Figures 3(b) and 3(c) show the pseudo phase and envelope spatial and temporal spectra, respectively. This phase again exhibits a typical spectrum of phase turbulence [21]. On the other hand, the spectrum density of the envelope follows the behavior close to $k^{-2.5}$ and ω^{-2} . Hence, the dynamics presented by local model Eq. (1) are qualitatively similar to those observed experimentally. However, the experiment is carried out far from the region where model Eq. (1) is valid since, in that region, the inherent fluctuations and imperfections of the experiment make the experimental study a thorny task.

Because the effect of the wavenumber of the pattern k_0 is dominant in the numerical simulation, we have filtered this wavelength from the spatial spectra. Figure 4(a) shows the spectrum of the scalar and pseudo phase and envelope field found when filtering. In this case, all the spectra tend to be close to k^{-2} . Alternatively, if one considers a bandstop filter [30], one obtains the result shown in Fig. 4(b). Again, one obtains spectra close to k^{-2} . Therefore, all these filters allow us to detect the complex aperiodic pattern dynamics of model Eq. (1).

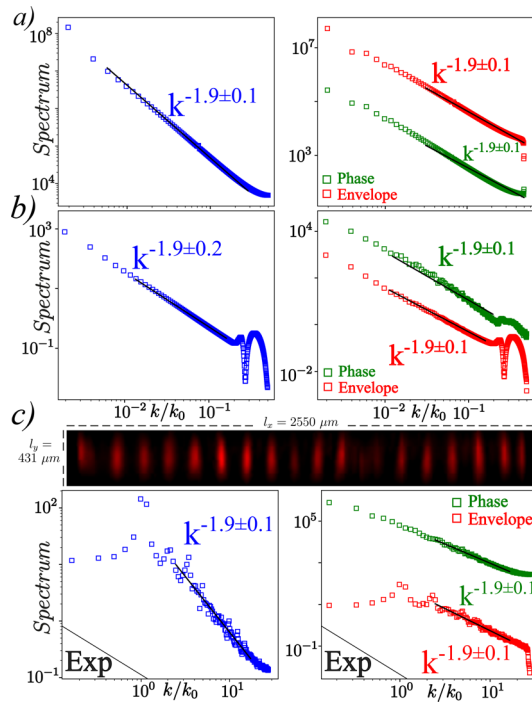


Fig. 4. Spatial spectrum densities. The spatial spectra of the scalar and pseudo phase and envelope field when (a) the pattern wavenumber k_0 is filtered in model Eq. (1), and (b) a Butterworth bandstop filter is applied to the pattern of model Eq. (1). (c) Spatial spectrum of the light intensity $I(x, t)$ (left panel) and the pseudo phase and envelope of the pattern (right panel) for an optical channel of dimensions $l_x = 2550 \mu\text{m}$ and $l_y = 431 \mu\text{m}$ with a voltage $V_0 = 8.48 \text{ Vrms}$. The points show the experimental results and the straight continuous curves help show the power law trend. Inset accounts for a snapshot of the observed pattern.

Experimentally, it is not possible to study a one-dimensional pattern; one always considers a quasi-one-dimensional system of dimensions $l_x \times l_y$ ($l_x = 1440 \mu\text{m}$, $l_x = 352 \mu\text{m}$, and $l_y \ll l_x$, $l_y/l_x \approx 0.24$). To study the effect of the aspect ratio l_y/l_x of the optical channel, we have decreased the aspect ratio by $l_x = 2550 \mu\text{m}$ and $l_y = 431 \mu\text{m}$ ($l_y/l_x \approx 0.17$). Unexpectedly, the tail of the spatial spectrum for the light intensity changes dramatically close to k^{-2} . Figure 4(c) illustrates the spatial spectrum density found. Likewise, we calculated the pseudo phase and envelope field associated with the pattern based on the Hilbert transform's analytical signal. Figure 4(c) summarizes the spectra found for these fields. Note that both spatial spectra present power laws close to -2 . Hence, quasi-dimensional dynamics can significantly impact the complex dynamics established by aperiodic patterns by altering the structure of defects, as shown in Figs. 1(b) and 4(c).

In conclusion, based on a liquid crystal light valve with optical feedback and a spatial light modulator, we have observed aperiodic one-dimensional patterns with temporal and spatial spectra with power laws. Likewise, through a valid mathematical model close to a Lifshitz point, we numerically find chaotic spatiotemporal patterns whose temporal

and spatial spectra have exponents similar to those observed experimentally.

Funding. ANID-Millennium Science Initiative 207 Program (ICN17_012); Fondo Nacional de Desarrollo Científico y Tecnológico (1210353).

Acknowledgment. The authors thank Y. Soupart for fruitful discussions.

Disclosures. The authors declare no conflicts of interest.

Data availability. Data underlying the results presented in this Letter are not publicly available at this time but may be obtained from the authors upon reasonable request.

REFERENCES

- L. M. Pismen, *Patterns and Interfaces in Dissipative Dynamics* (Springer, 2006).
- M. Cross and H. Greenside, *Pattern Formation and Dynamics in Non-Equilibrium Systems* (Cambridge University Press, 2009).
- F. T. Arecchi, S. Boccaletti, and P. Ramazza, *Phys. Rep.* **318**, 1 (1999).
- D. Dangoisse, D. Hennequin, C. Lepers, *et al.*, *Phys. Rev. A* **46**, 5955 (1992).
- G. Huyet, M. C. Martinoni, J. R. Tredicce, *et al.*, *Phys. Rev. Lett.* **75**, 4027 (1995).
- A. Bartolo, N. Vigne, M. Marconi, *et al.*, *Optica* **9**, 1386 (2022).
- C. Denz, M. Schwab, and C. Weillnau, *Transverse-Pattern Formation in Photorefractive Optics* (Springer, 2003).
- T. Ackemann and W. Lange, *Phys. Rev. A* **50**, R4468 (1994).
- G. Agez, P. Glorieux, M. Taki, *et al.*, *Phys. Rev. A* **74**, 043814 (2006).
- S. Residori, *Phys. Rep.* **416**, 201 (2005).
- M. G. Clerc, G. González-Cortés, V. Odent, *et al.*, *Opt. Express* **24**, 15478 (2016).
- E. G. Turitsyna, S. V. Smirnov, S. Sugavanam, *et al.*, *Nat. Photonics* **7**, 783 (2013).
- I. R. R. Gonzalez, B. C. Lima, P. I. R. Pincheira, *et al.*, *Nat. Commun.* **8**, 15731 (2017).
- G. Xu, D. Vocke, D. Faccio, *et al.*, *Nat. Commun.* **6**, 8131 (2015).
- P. J. Aguilera-Rojas, M. G. Clerc, S. Echeverria-Alar, *et al.*, *Chaos, Solitons Fractals* **182**, 114851 (2024).
- R. Alert, J. Casademunt, and J. F. Joanny, *Annu. Rev. Condens Matter Phys.* **13**, 143 (2022).
- K. A. Takeuchi and M. Sano, *Phys. Rev. Lett.* **104**, 230601 (2010).
- Q. Ouyang and H. L. Swinney, *Chaos* **1**, 411 (1991).
- S. Ghashghaie, W. Breymann, J. Peinke, *et al.*, *Nature* **381**, 767 (1996).
- E. A. L. Henn, J. A. Seman, G. Roati, *et al.*, *Phys. Rev. Lett.* **103**, 045301 (2009).
- Y. Kuramoto, *Chemical Oscillations, Waves, and Turbulence*, Springer Series in Synergetics (Springer, 1984).
- J. Claerbout, *Fundamentals of Geophysical Data Processing* (McGraw-Hill, 1976).
- M. G. Clerc and N. Verschueren, *Phys. Rev. E* **88**, 052916 (2013).
- D. E. Sigeti, *Phys. Rev. E* **52**, 2443 (1995).
- M. Bertram, C. Beta, M. Pollmann, *et al.*, *Phys. Rev. E* **67**, 036208 (2003).
- C. Y. Zenkova, M. P. Gorsky, and P. A. Ryabiy, *Opt. Appl.* **46**, 153 (2016).
- U. Frisch, *Turbulence: The Legacy of AN Kolmogorov* (Cambridge University Press, 1995).
- M. G. Clerc, A. Petrossian, and S. Residori, *Phys. Rev. E* **71**, 015205 (2005).
- A. J. Alvarez-Socorro, M. G. Clerc, G. González-Cortés, *et al.*, *Phys. Rev. E* **95**, 010202 (2017).
- S. Butterworth, *Wireless Engineer* **7**, 536 (1930).